562 global impact fluxes and mean velocity of the impacting projectiles on Mercury (Le Feuvre and
563 Wieczorek 2008) could potentially contribute to higher crustal porosities on Mercury than the
564 Moon.
565 High crustal porosities are observed across heavily cratered regions. Impact events fracture the
566 crust, yielding the generation of additional pore space (Reynolds 1885). A longer history of
567 bombardment generally results in higher porosity. Low porosities are detected across the NVP,
568 where impact bombardments after their formation ~4 Gy ago strongly affected their bulk density
569 (Frank et al. 2017; Whitten et al. 2014). A region located within $210-240°E$ longitudes and $60-$
570 $80°N$ latitudes that is characterized by high crater densities (*i.e.*, *N(20)* >150 per million km^2)
571 shows 10% porosities. Preexisting high porosity in the crust across this heavily cratered province
572 may have led to the compaction of the pore space for some impacts, which may lead to equilibrium
573 porosity after sufficient bombardment (Milbury et al. 2015).

574 ## 5. Conclusions

575 The enhanced spatial resolution of Mercury's gravity field *HgM009* allowed us to study the
576 properties of the crust and lithosphere by using localized spectral admittance analyses. Compared
577 to the accuracy of other celestial bodies' gravity field, as, for example, the Moon and Mars, our
578 knowledge of the short wavelength anomalies is still limited to a few regions of the northern
579 hemisphere. The resolution of the gravity field is between spherical harmonic degrees 80 and 160
580 across the mid-northern latitudes. The gravity signal associated with those harmonics is caused by
581 different sources, including the crustal density and thickness variations, and the flexure of the
582 lithosphere.
583 To estimate the crust and lithospheric properties, we used a method that uses the combination of
584 localized admittance spectra and predictions based on a lithospheric flexural model (Turcotte et al.

585 1981). The crustal density and thickness, and the elastic thickness are adjusted as free parameters
586 to obtain a good fit between the measured and predicted spectra. Crustal thickness variations that
587 are not associated with flexure are not included in our modeling, limiting our interpretation
588 regarding local variations of the crustal thickness. The parameter that is best constrained in our
589 analysis is the bulk density, and a map of its lateral variations (Figure 13) provides key information
590 on the crustal porosity (Figure 14).
591 An accurate fit between measured and predicted admittance spectra is obtained across a few
592 regions of Mercury's northern hemisphere, including the high-Mg province, the NVP, and the IcP.
593 This may result from the resolution of the gravity field that is still limited at lower latitudes.
594 Furthermore, the theoretical model adopted in our study accounts for top-loading only. Surface
595 and subsurface load modeling (e.g., Grott and Wieczorek 2012; Broquet and Wieczorek 2019)
596 may help to enhance the admittance fit between measurements and predictions. This transfer
597 function, however, is often based on the assumption that the ratio of surface to subsurface loads is
598 constant for all degrees (*e.g.*, Broquet and Wieczorek 2019), which would not be well-suited for
599 the entire northern hemisphere.
600 The map of the bulk density is combined with the map of the grain density (Namur and Charlier
601 2017; Beuthe et al. 2020) to yield the lateral variations of the upper crust porosity. Higher crustal
602 porosities are observed across the high-Mg region.
603 To investigate the crust and lithosphere in the southern hemisphere, accurate measurements of
604 gravity and topography will be acquired by the ESA mission BepiColombo that will be orbiting
605 Mercury from December 2025 (Genova et al. 2021). Mercury's gravity field will be estimated
606 globally to spherical harmonics degree and order 50-60. The method proposed in this study will

607 then be used to analyze gravity/topography admittance spectra, enabling geophysical constraints
608 on the properties of the crust in the southern hemisphere.
609

610 ## Acknowledgements

611 The gravity field *HgM009* and the ancillary information, including the covariance matrix,
612 presented in this study are archived at https://sites.google.com/uniroma1.it/spring. Our software
613 that enables localized spectral analyses of gravity/topography correlation and admittance is based
614 on the free software package *shtools* (Wieczorek and Meschede 2018). We are grateful to Walter
615 S. Kiefer and an anonymous reviewer for helpful and constructive comments on previous versions
616 of this paper. AG acknowledges funding from the *Rita Levi Montalcini Programme* of the Italian
617 Ministry of University and Research (MUR).

References

Becker, Kris J, Mark S Robinson, Tammy L Becker, Lynn A Weller, Kenneth L Edmundson, Gregory A Neumann, Mark E Perry, and Sean C Solomon. 2016. "First Global Digital Elevation Model of Mercury." In *Presented at the 47th Lunar and Planetary Science Conference*. Houston, TX: Lunar and Planetary Institute.

Beuthe, Mikael, Bernard Charlier, Olivier Namur, Attilio Rivoldini, and Tim van Hoolst. 2020. "Mercury's Crustal Thickness Correlates With Lateral Variations in Mantle Melt Production." *Geophysical Research Letters* 47 (9): e2020GL087261. https://doi.org/10.1029/2020GL087261.

Broquet, A., and M. A. Wieczorek. 2019. "The Gravitational Signature of Martian Volcanoes." *Journal of Geophysical Research: Planets* 124 (8): 2054–86. https://doi.org/10.1029/2019JE005959.

Byrne, Paul K., Lillian R. Ostrach, Caleb I. Fassett, Clark R. Chapman, Brett W. Denevi, Alexander J. Evans, Christian Klimczak, Maria E. Banks, James W. Head, and Sean C. Solomon. 2016. "Widespread Effusive Volcanism on Mercury Likely Ended by about 3.5 Ga." *Geophysical Research Letters* 43 (14): 7408–16. https://doi.org/10.1002/2016GL069412.

Charlier, Bernard, Timothy L. Grove, and Maria T. Zuber. 2013. "Phase Equilibria of Ultramafic Compositions on Mercury and the Origin of the Compositional Dichotomy." *Earth and Planetary Science Letters* 363 (February): 50–60. https://doi.org/10.1016/J.EPSL.2012.12.021.

Charlier, Bernard, and Olivier Namur. 2019. "The Origin and Differentiation of Planet Mercury." *Elements* 15 (1): 9–14. https://doi.org/10.2138/GSELEMENTS.15.1.9.

Denevi, B.W., C.M. Ernst, L.M. Prockter, and M.S. Robinson. 2018. "The Geologic History of Mercury'." In *Mercury*, edited by Sean C. Solomon, Larry R. Nittler, and Brian J. Anderson, 144–75. Cambridge University Press (2018). https://doi.org/10.1017/9781316650684.

Ermakov, A. I., R. S. Park, and B. G. Bills. 2018. "Power Laws of Topography and Gravity Spectra of the Solar System Bodies." *Journal of Geophysical Research: Planets* 123 (8): 2038–64. https://doi.org/10.1029/2018JE005562.

Fassett, C I, S J Kadish, J W Head, S C Solomon, and R G Strom. 2011. "The Global Population of Large Craters on Mercury and Comparison with the Moon." *Wiley Online Library* 38 (10): 10202. https://doi.org/10.1029/2011GL047294.

Frank, Elizabeth A., Ross W.K. Potter, Oleg Abramov, Peter B. James, Rachel L. Klima, Stephen J. Mojzsis, and Larry R. Nittler. 2017. "Evaluating an Impact Origin for Mercury's High-Magnesium Region." *Journal of Geophysical Research: Planets* 122 (3): 614–32. https://doi.org/10.1002/2016JE005244.

Genova, A., S. Goossens, E. Mazarico, F.G. Lemoine, G.A. Neumann, W. Kuang, T.J. Sabaka, et al. 2019. "Geodetic Evidence That Mercury Has A Solid Inner Core." *Geophysical Research Letters* 46 (7). https://doi.org/10.1029/2018GL081135.

Genova, A., L. Iess, and M. Marabucci. 2013. "Mercury's Gravity Field from the First Six Months of MESSENGER Data." *Planetary and Space Science* 81 (June): 55–64. https://doi.org/10.1016/J.PSS.2013.02.006.

Genova, A., E. Mazarico, S. Goossens, F.G. Lemoine, G.A. Neumann, D.E. Smith, and M.T. Zuber. 2018. "Solar System Expansion and Strong Equivalence Principle as Seen by the

NASA MESSENGER Mission." *Nature Communications* 9 (1). https://doi.org/10.1038/s41467-017-02558-1.

Genova, Antonio, Hauke Hussmann, Tim Van Hoolst, Daniel Heyner, Luciano Iess, Francesco Santoli, Nicolas Thomas, et al. 2021. "Geodesy, Geophysics and Fundamental Physics Investigations of the BepiColombo Mission." *Space Science Reviews 2021 217:2* 217 (2): 1–62. https://doi.org/10.1007/S11214-021-00808-9.

Goossens, S., A. Genova, P. B. James, and E. Mazarico. 2022. "Estimation of Crust and Lithospheric Properties for Mercury from High-resolution Gravity and Topography." *The Planetary Science Journal* 3(6): 145. https://doi.org/10.3847/PSJ/ac703f.

Goossens, S., T.J. Sabaka, A. Genova, E. Mazarico, J.B. Nicholas, and G.A. Neumann. 2017. "Evidence for a Low Bulk Crustal Density for Mars from Gravity and Topography." *Geophysical Research Letters* 44 (15). https://doi.org/10.1002/2017GL074172.

Grott, M., and M. A. Wieczorek. 2012. "Density and Lithospheric Structure at Tyrrhena Patera, Mars, from Gravity and Topography Data." *Icarus* 221 (1): 43–52. https://doi.org/10.1016/J.ICARUS.2012.07.008.

Hauck, Steven A., Andrew J. Dombard, Roger J. Phillips, and Sean C. Solomon. 2004. "Internal and Tectonic Evolution of Mercury." *Earth and Planetary Science Letters* 222 (3–4): 713–28. https://doi.org/10.1016/J.EPSL.2004.03.037.

James, Peter B., Maria T. Zuber, Roger J. Phillips, and Sean C. Solomon. 2015. "Support of Long-Wavelength Topography on Mercury Inferred from MESSENGER Measurements of Gravity and Topography." *Journal of Geophysical Research: Planets* 120 (2): 287–310. https://doi.org/10.1002/2014JE004713.

Kaula, W.M. 1966. *Theory of Satellite Geodesy. Applications of Satellites to Geodesy*. Waltham, MA: Blaisdell Publishing Company.

Kay, Jonathan P., and Andrew J. Dombard. 2019. "Long-Wavelength Topography on Mercury Is Not from Folding of the Lithosphere." *Icarus* 319 (February): 724–28. https://doi.org/10.1016/J.ICARUS.2018.09.040.

Klima, Rachel L., Brett W. Denevi, Carolyn M. Ernst, Scott L. Murchie, and Patrick N. Peplowski. 2018. "Global Distribution and Spectral Properties of Low-Reflectance Material on Mercury." *Geophysical Research Letters* 45 (7): 2945–53. https://doi.org/10.1002/2018GL077544.

Klimczak, Christian. 2015. "Limits on the Brittle Strength of Planetary Lithospheres Undergoing Global Contraction." *Journal of Geophysical Research: Planets* 120 (12): 2135–51. https://doi.org/10.1002/2015JE004851.

Konopliv, A. S., W. B. Banerdt, and W. L. Sjogren. 1999. "Venus Gravity: 180th Degree and Order Model." *Icarus* 139 (1): 3–18. https://doi.org/10.1006/ICAR.1999.6086.

Konopliv, A. S., R. S. Park, and A. I. Ermakov. 2020. "The Mercury Gravity Field, Orientation, Love Number, and Ephemeris from the MESSENGER Radiometric Tracking Data." *Icarus* 335 (January): 113386. https://doi.org/10.1016/J.ICARUS.2019.07.020.

Le Feuvre, M., and M.A. Wieczorek. 2008. "Nonuniform Cratering of the Terrestrial Planets." *Icarus* 197 (1): 291–306. https://doi.org/10.1016/J.ICARUS.2008.04.011.

Marchi, Simone, Clark R. Chapman, Caleb I. Fassett, James W. Head, W. F. Bottke, and Robert G. Strom. 2013. "Global Resurfacing of Mercury 4.0–4.1 Billion Years Ago by Heavy Bombardment and Volcanism." *Nature 2013 499:7456* 499 (7456): 59–61. https://doi.org/10.1038/nature12280.

Margot, Jean-Luc, Stanton J. Peale, Sean C. Solomon, Steven A. Hauck, Frank D. Ghigo, Raymond F. Jurgens, Marie Yseboodt, Jon D. Giorgini, Sebastiano Padovan, and Donald B. Campbell. 2012. "Mercury's Moment of Inertia from Spin and Gravity Data." *Journal of Geophysical Research: Planets* 117 (E12): 0–09. https://doi.org/10.1029/2012JE004161.

Mazarico, E., A. Genova, S. Goossens, F.G. Lemoine, G.A. Neumann, M.T. Zuber, D.E. Smith, and S.C. Solomon. 2014. "The Gravity Field, Orientation, and Ephemeris of Mercury from MESSENGER Observations after Three Years in Orbit." *Journal of Geophysical Research: Planets* 119 (12). https://doi.org/10.1002/2014JE004675.

Melosh, J.H. 1977. "Global Tectonics of a Despun Planet." *Icarus* 31 (2): 221–43. https://doi.org/10.1016/0019-1035(77)90035-5.

Milbury, C., B. C. Johnson, H. J. Melosh, G. S. Collins, D. M. Blair, J. M. Soderblom, F. Nimmo, C. J. Bierson, R. J. Phillips, and M. T. Zuber. 2015. "Preimpact Porosity Controls the Gravity Signature of Lunar Craters." *Geophysical Research Letters* 42 (22): 9711–16. https://doi.org/10.1002/2015GL066198.

Murchie, Scott L., Rachel L. Klima, Brett W. Denevi, Carolyn M. Ernst, Mary R. Keller, Deborah L. Domingue, David T. Blewett, et al. 2015. "Orbital Multispectral Mapping of Mercury with the MESSENGER Mercury Dual Imaging System: Evidence for the Origins of Plains Units and Low-Reflectance Material." *Icarus* 254 (July): 287–305. https://doi.org/10.1016/J.ICARUS.2015.03.027.

Namur, Olivier, and Bernard Charlier. 2017. "Silicate Mineralogy at the Surface of Mercury." https://doi.org/10.1038/NGEO2860.

Namur, Olivier, Max Collinet, Bernard Charlier, Timothy L. Grove, Francois Holtz, and Catherine McCammon. 2016. "Melting Processes and Mantle Sources of Lavas on Mercury." *Earth and Planetary Science Letters* 439 (April): 117–28. https://doi.org/10.1016/J.EPSL.2016.01.030.

Peplowski, Patrick N, Rachel L Klima, David J Lawrence, Carolyn M Ernst, Brett W Denevi, Elizabeth A Frank, John O Goldsten, Scott L Murchie, Larry R Nittler, and Sean C Solomon. 2016. "Remote Sensing Evidence for an Ancient Carbon-Bearing Crust on Mercury" 9: 273–76. https://doi.org/10.1038/NGEO2669.

Reynolds, Osborne. 1885. " LVII. On the Dilatancy of Media Composed of Rigid Particles in Contact. With Experimental Illustrations ." *The London, Edinburgh, and Dublin Philosophical Magazine and Journal of Science* 20 (127): 469–81. https://doi.org/10.1080/14786448508627791.

Schlemm, Charles E., Richard D. Starr, George C. Ho, Kathryn E. Bechtold, Sarah A. Hamilton, John D. Boldt, William V. Boynton, et al. 2007. "The X-Ray Spectrometer on the MESSENGER Spacecraft." *The Messenger Mission to Mercury*, 393–415. https://doi.org/10.1007/978-0-387-77214-1_11.

Smith, David E., Maria T. Zuber, Roger J. Phillips, Sean C. Solomon, Steven A. Hauck, Frank G. Lemoine, Erwan Mazarico, et al. 2012. "Gravity Field and Internal Structure of Mercury from MESSENGER." *Science* 336 (6078): 214–17. https://doi.org/10.1126/SCIENCE.1218809.

Solomon, Sean C., Ralph L. McNutt, Robert E. Gold, Mario H. Acuña, Daniel N. Baker, William V. Boynton, Clark R. Chapman, et al. 2001. "The MESSENGER Mission to Mercury: Scientific Objectives and Implementation." *Planetary and Space Science* 49 (14–15): 1445–65. https://doi.org/10.1016/S0032-0633(01)00085-X.

Solomon, Sean C., Larry R. Nittler, and Brian J. Anderson, eds. 2018. *Mercury: The View after MESSENGER*. Vol. 21. Cambridge, UK: Cambridge University Press.

Sori, Michael M. 2018. “A Thin, Dense Crust for Mercury.” *Earth and Planetary Science Letters* 489 (May): 92–99. https://doi.org/10.1016/J.EPSL.2018.02.033.

Strom, Robert G., Maria E. Banks, Clark R. Chapman, Caleb I. Fassett, Jeffrey A. Forde, James W. Head, William J. Merline, Louise M. Prockter, and Sean C. Solomon. 2011. “Mercury Crater Statistics from MESSENGER Flybys: Implications for Stratigraphy and Resurfacing History.” *Planetary and Space Science* 59 (15): 1960–67. https://doi.org/10.1016/J.PSS.2011.03.018.

Tapley, Byron D., Bob E. Schutz, and George H. Born. 2004. *Statistical Orbit Determination*. *Statistical Orbit Determination*. Elsevier Inc. https://doi.org/10.1016/B978-0-12-683630-1.X5019-X.

Trask, Newell J., and John E. Guest. 1975. “Preliminary Geologic Terrain Map of Mercury.” *Journal of Geophysical Research* 80 (17): 2461–77. https://doi.org/10.1029/JB080I017P02461.

Turcotte, D. L., R. J. Willemann, W. F. Haxby, and John Norberry. 1981. “Role of Membrane Stresses in the Support of Planetary Topography.” *Journal of Geophysical Research: Solid Earth* 86 (B5): 3951–59. https://doi.org/10.1029/JB086IB05P03951.

Vander Kaaden, Kathleen E., and Francis M. McCubbin. 2015. “Exotic Crust Formation on Mercury: Consequences of a Shallow, FeO-Poor Mantle.” *Journal of Geophysical Research: Planets* 120 (2): 195–209. https://doi.org/10.1002/2014JE004733.

Verma, Ashok Kumar, and Jean-Luc Margot. 2016. “Mercury’s Gravity, Tides, and Spin from MESSENGER Radio Science Data.” *Journal of Geophysical Research: Planets* 121 (9): 1627–40. https://doi.org/10.1002/2016JE005037.

Weider, Shoshana Z., Larry R. Nittler, Richard D. Starr, Ellen J. Crapster-Pregont, Patrick N. Peplowski, Brett W. Denevi, James W. Head, et al. 2015. “Evidence for Geochemical Terranes on Mercury: Global Mapping of Major Elements with MESSENGER’s X-Ray Spectrometer.” *Earth and Planetary Science Letters* 416 (April): 109–20. https://doi.org/10.1016/J.EPSL.2015.01.023.

Weider, Shoshana Z., Larry R. Nittler, Richard D. Starr, Timothy J. McCoy, Karen R. Stockstill-Cahill, Paul K. Byrne, Brett W. Denevi, James W. Head, and Sean C. Solomon. 2012. “Chemical Heterogeneity on Mercury’s Surface Revealed by the MESSENGER X-Ray Spectrometer.” *Journal of Geophysical Research: Planets* 117 (E12): 0–05. https://doi.org/10.1029/2012JE004153.

Whitten, Jennifer L., James W. Head, Brett W. Denevi, and Sean C. Solomon. 2014. “Intercrater Plains on Mercury: Insights into Unit Definition, Characterization, and Origin from MESSENGER Datasets.” *Icarus* 241 (October): 97–113. https://doi.org/10.1016/J.ICARUS.2014.06.013.

Wieczorek, Mark A. 2015. “The Gravity and Topography of the Terrestrial Planets.” In *Treatise on Geophysics*.

Wieczorek, Mark A., and Matthias Meschede. 2018. “SHTools: Tools for Working with Spherical Harmonics.” *Geochemistry, Geophysics, Geosystems* 19 (8): 2574–92. https://doi.org/10.1029/2018GC007529.

Wieczorek, Mark A., Gregory A. Neumann, Francis Nimmo, Walter S. Kiefer, G. Jeffrey Taylor, H. Jay Melosh, Roger J. Phillips, et al. 2013. “The Crust of the Moon as Seen by GRAIL.” *Science* 339 (6120): 671–75. https://doi.org/10.1126/SCIENCE.1231530.

Wieczorek, Mark A., and Frederik J. Simons. 2005. “Localized Spectral Analysis on the Sphere.” *Geophysical Journal International* 162 (3): 655–75. https://doi.org/10.1111/J.1365-246X.2005.02687.X/2/162-3-655-FIG011.JPEG.

Zuber, Maria T., David E. Smith, Roger J. Phillips, Sean C. Solomon, Gregory A. Neumann, Steven A. Hauck, Stanton J. Peale, et al. 2012. “Topography of the Northern Hemisphere of Mercury from MESSENGER Laser Altimetry.” *Science* 336 (6078): 217–20. https://doi.org/10.1126/SCIENCE.1218805.

Tables

Table 1 Lower and upper limits, and step size of the parameters of interest that are used in the global theoretical admittance function (Eqs. 3 and 4).

Parameter	Lower Bound	Upper Bound	Step Size
Crustal density ρ_c (kg m^{-3})	2200	3200	5
Crustal thickness T_c (km)	0	200	5
Elastic thickness T_e (km)	0	200	5

Figures

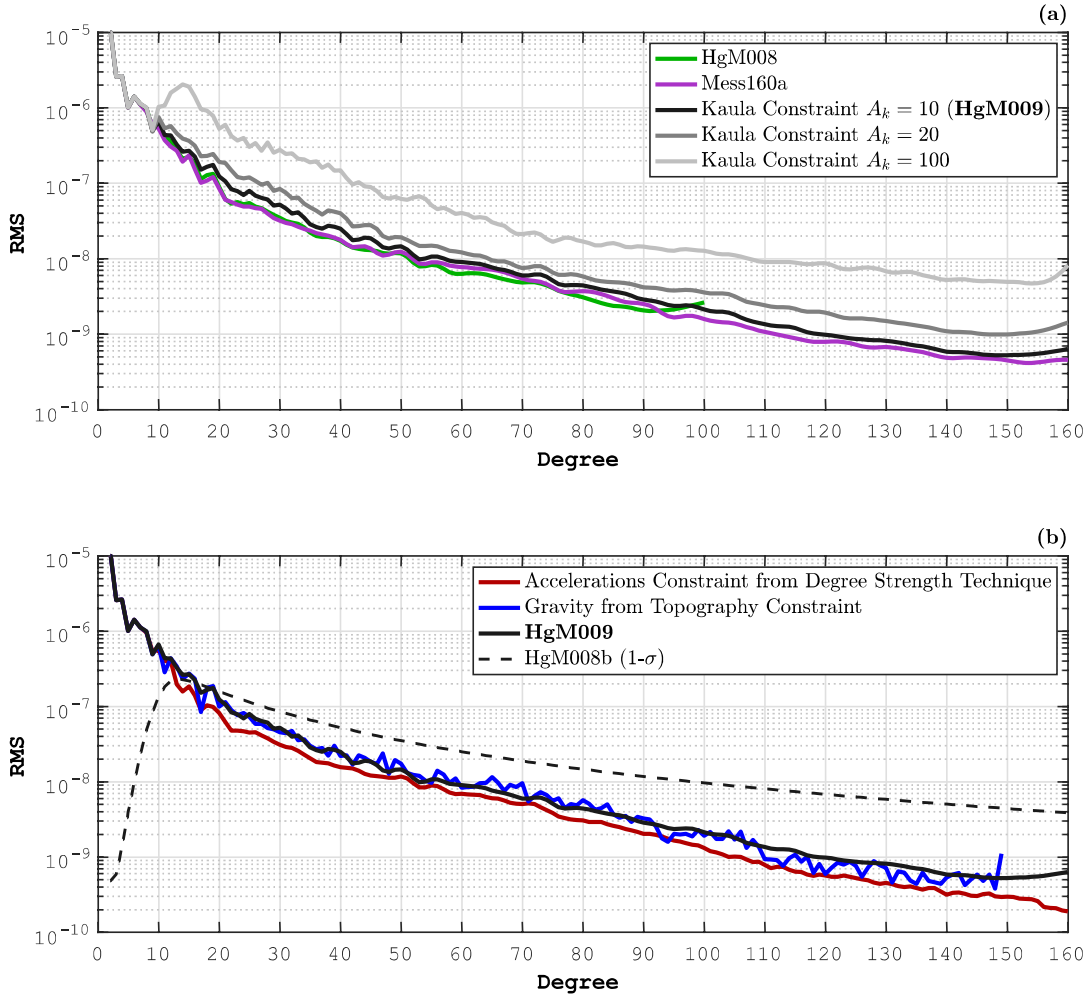

Figure 1 Power spectra of the gravity solutions obtained by using an *a priori* constraint based on (**a**) the Kaula rule with different A_k parameters and (**b**) the degree strength map (**red**) and the gravity from topography (**blue**). The gravity solution, *HgM009*, is expanded to degree and order 160 and is retrieved with a looser Kaula constraint (A_k=10) compared to the latest solutions *HgM008* (**green**) and *Mess160a* (**purple**).

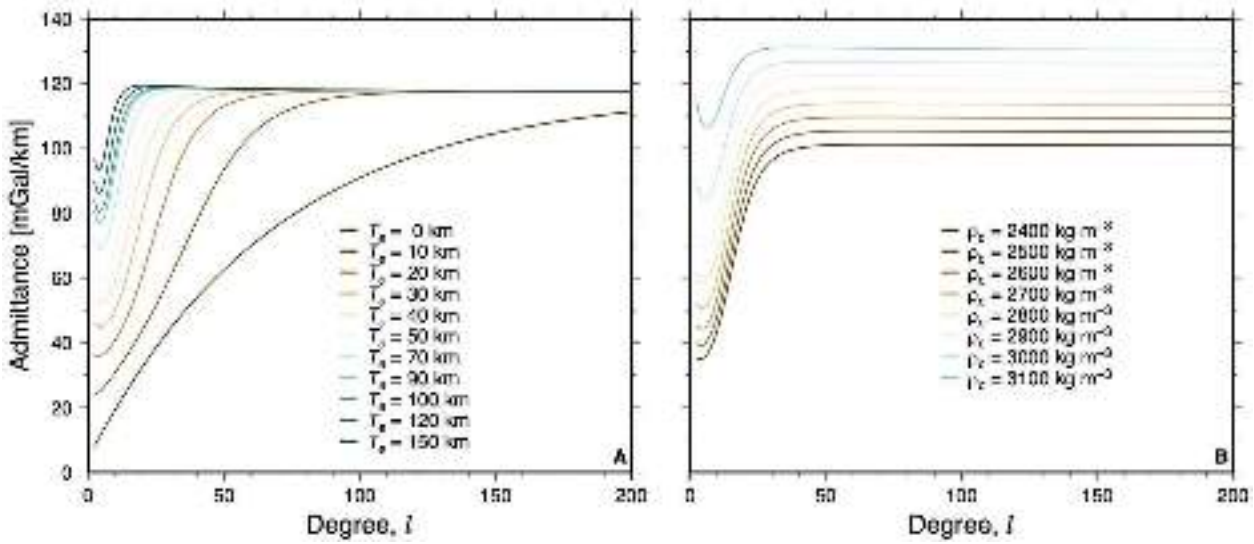

Figure 2 (**A**) Global gravity/topography admittances for crustal thickness and density of 35 km and 2800 kg m^{-3}, respectively. (**B**) Global gravity/topography admittances for crustal and elastic thickness of 35 km and 50 km, respectively.

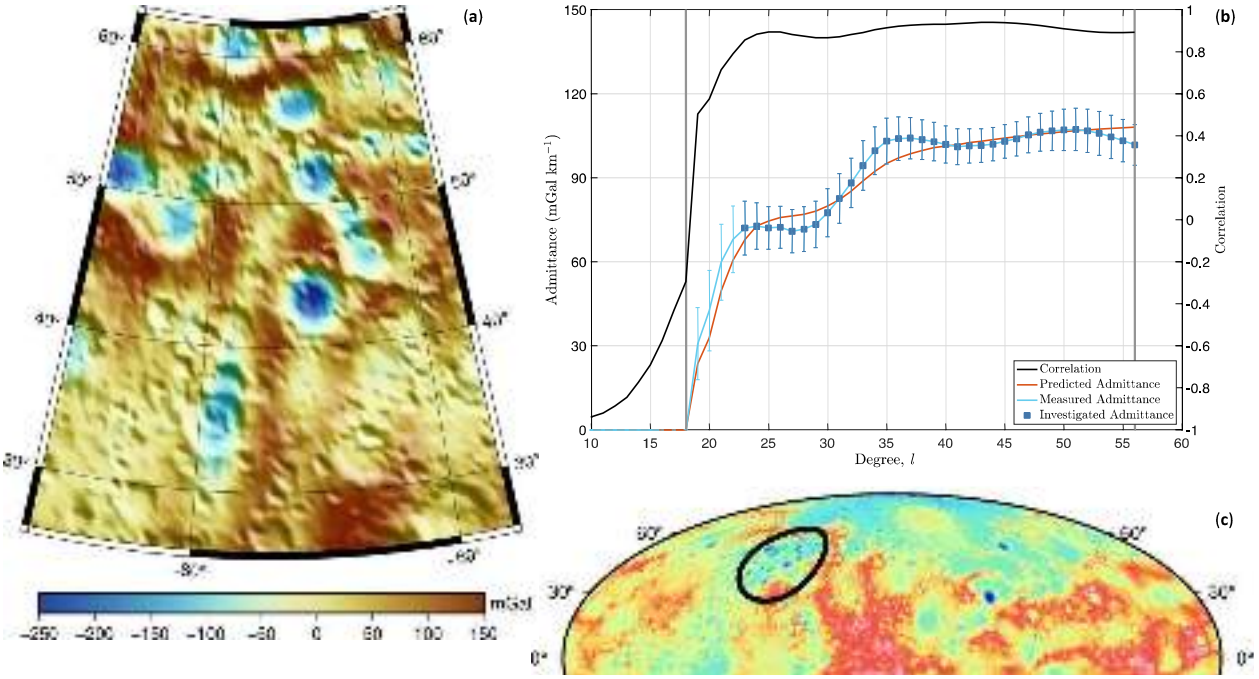

Figure 3 (**a**) Local map of free-air gravity anomaly (mGal) shown over shaded topographic relief in a Lambert Conformal Conic projection, and (**b**) correlation and admittance between gravity and topography localized on (**c**) a spherical cap centered at 286°E longitude and 44°N latitude. The localization windowing is carried out with a 18° radius, a concentration factor of 0.999 ($L_{win} = 18$), and a spherical harmonic expansion to degree $l_{max} = 74$. The measured admittance is compared to the predicted admittance spectra based on the surface loading model presented in Sec. 2.3. The investigated admittance spectrum includes spherical harmonic degrees that provides a signal to noise ratio larger than (correlation $\gamma(l)$>0.816). The vertical gray lines show the range of spherical harmonic degrees between L_{win} and $l_{max} - L_{win} = l_{DS}$, where l_{DS} is the degree resolution resulting from the degree strength map (Figure S1).

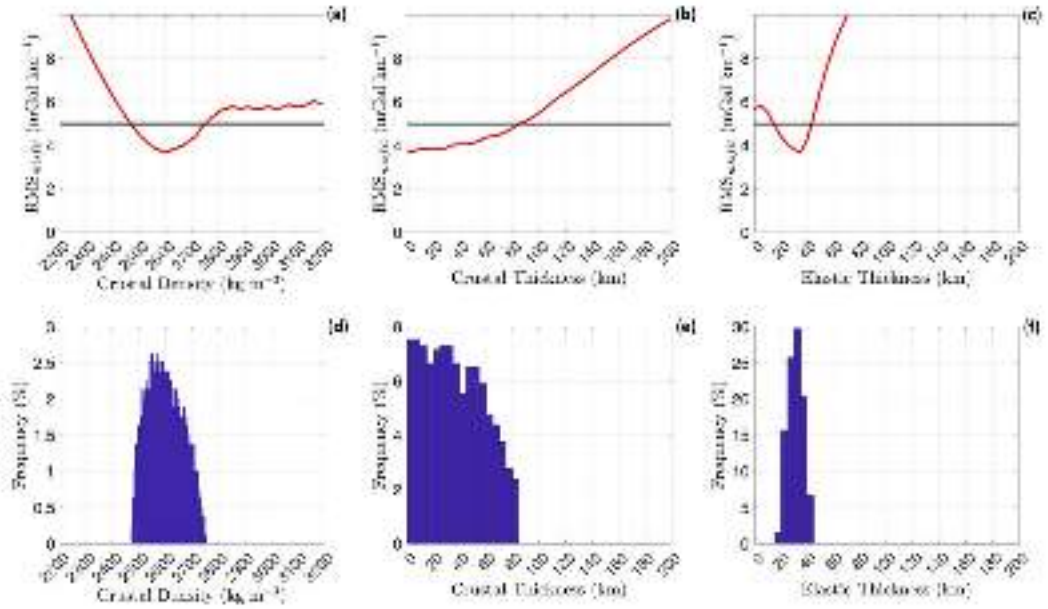

Figure 4 (**a-b-c**) Misfit plots and (**d-e-f**) histograms for the crustal density and thickness, and elastic thickness resulting from the comparison between measured and predicted localized admittance shown in Figure 3-b. The black horizontal line shows the RMS of the formal uncertainties of the local admittance, $\overline{\sigma}$, and the red curve the RMS_{misfit}as function of the estimated parameter.

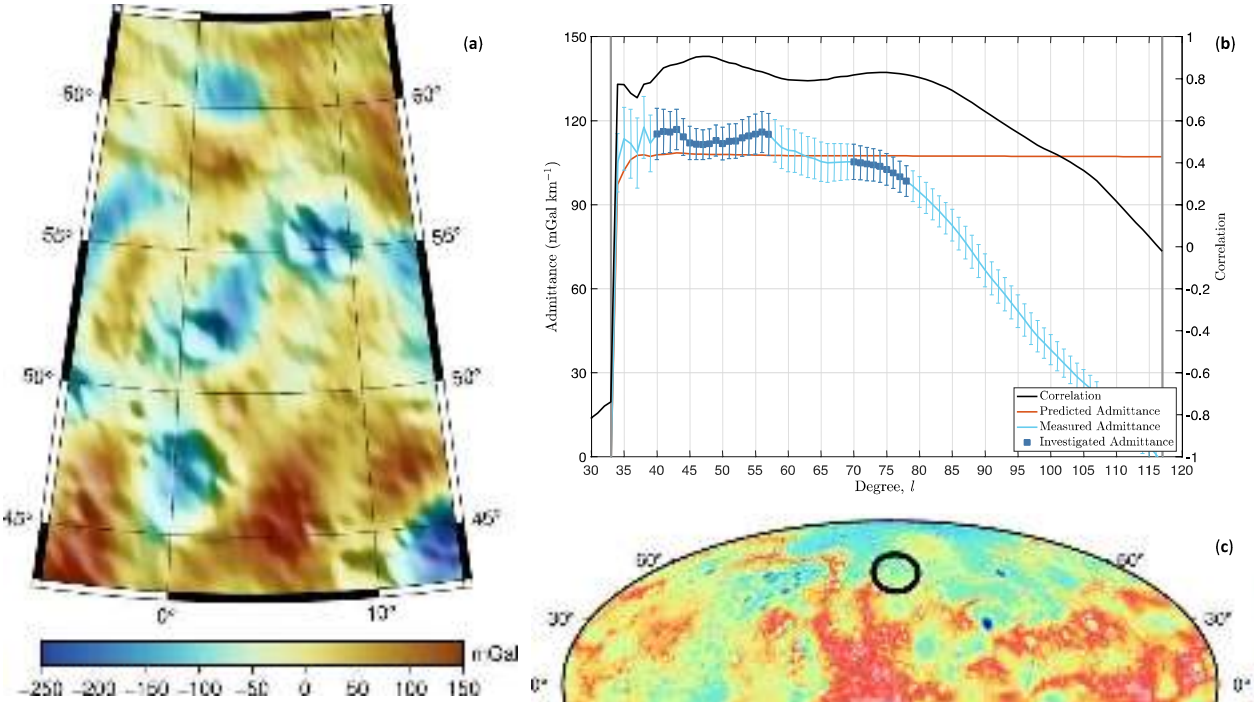

Figure 5 (**a**) Local map of free-air gravity anomaly (mGal) shown over shaded topographic relief in a Lambert Conformal Conic projection, and (**b**) correlation and admittance between gravity and topography localized on (**c**) a spherical cap centered at 4°E longitude and 53°N latitude. The localization windowing is carried out with a 10° radius, a concentration factor of 0.999 ($L_{win} = 33$), and a spherical harmonic expansion to degree $l_{max} = 148$ (see caption of Figure 3 for more details).

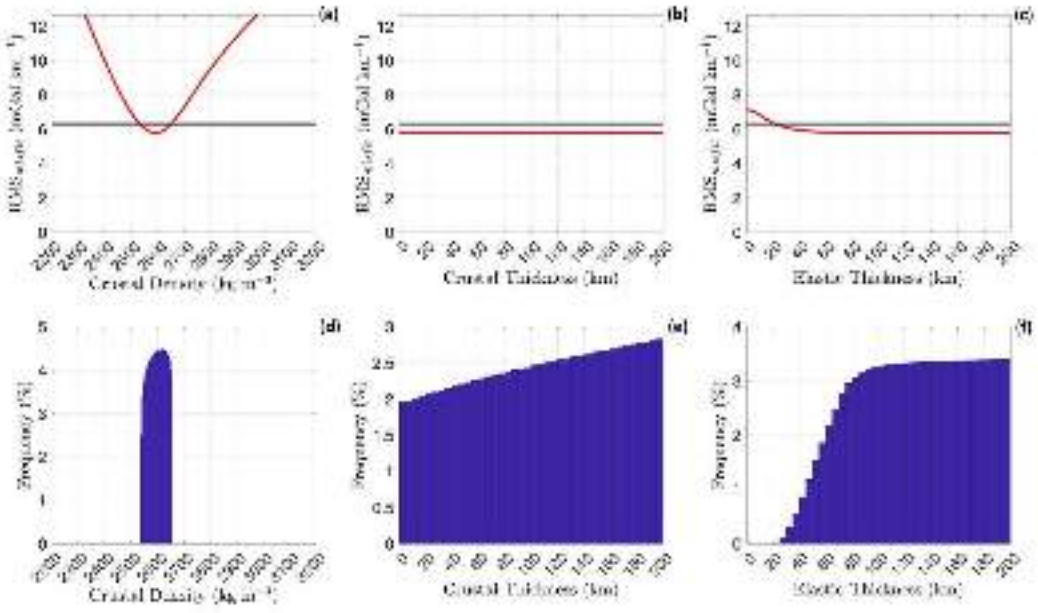

Figure 6 (**a-b-c**) Misfit plots and (**d-e-f**) histograms for the crustal density and thickness, and elastic thickness resulting from the comparison between measured and predicted localized admittance shown in Figure 5-b. The black horizontal line shows the RMS of the formal uncertainties of the local admittance, $\overline{\sigma}$, and the red curve the RMS_{misfit}as function of the estimated parameter.

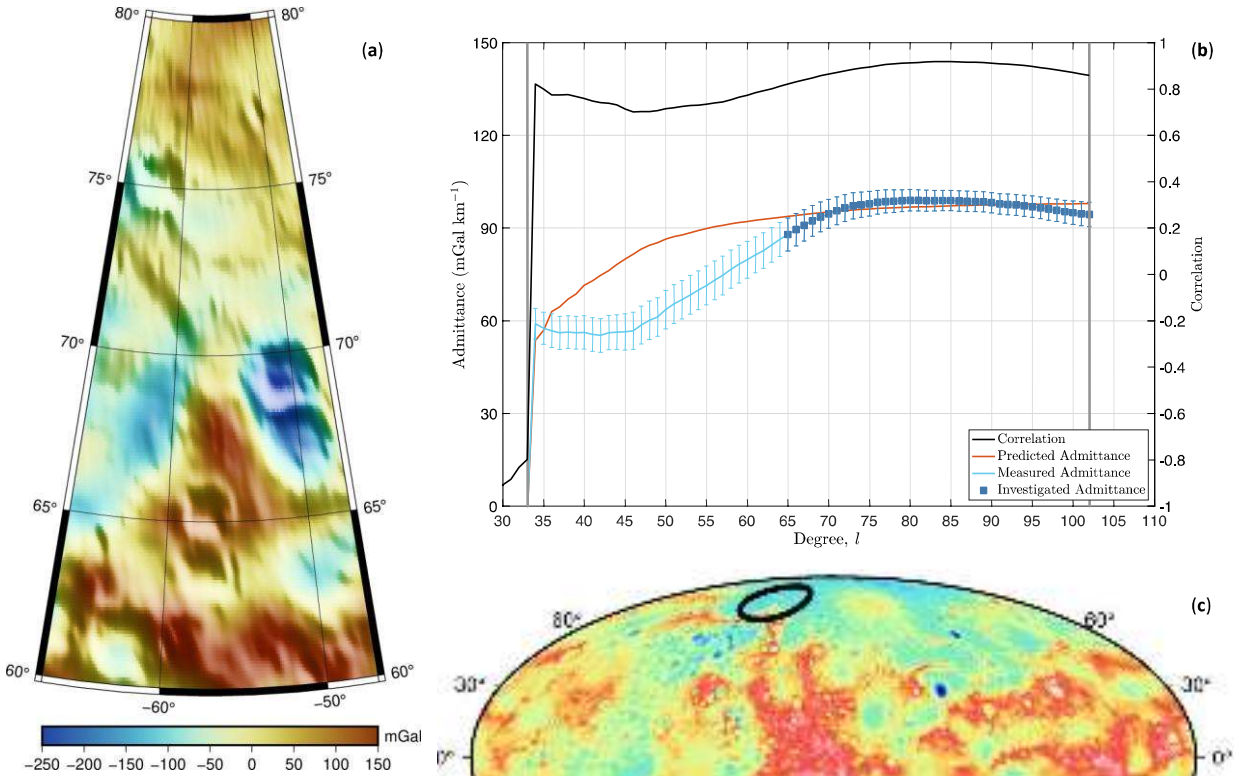

Figure 7 (**a**) Local map of free-air gravity anomaly (mGal) shown over shaded topographic relief in a Lambert Conformal Conic projection, and (**b**) correlation and admittance between gravity and topography localized on (**c**) a spherical cap centered at 303°E longitude and 70°N latitude. The localization windowing is carried out with a 10° radius, a concentration factor of 0.999 ($L_{win} = 33$), and a spherical harmonic expansion to degree $l_{max} = 135$ (see caption of Figure 3 for more details).

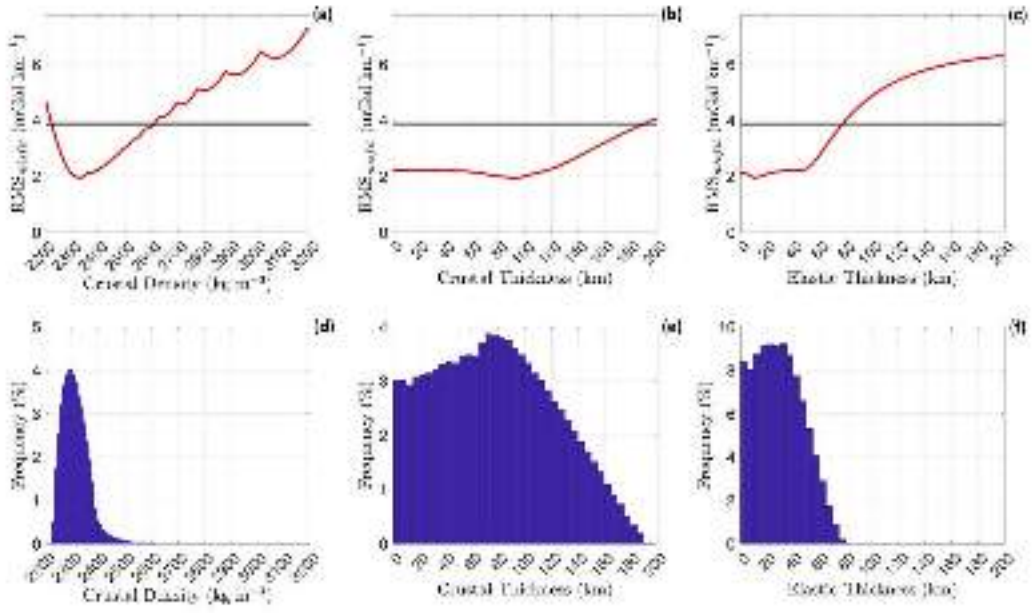

Figure 8 (**a-b-c**) Misfit plots and (**d-e-f**) histograms for the crustal density and thickness, and elastic thickness resulting from the comparison between measured and predicted localized admittance shown in Figure 7-b. The black horizontal line shows the RMS of the formal uncertainties of the local admittance, $\overline{\sigma}$, and the red curve the RMS_{misfit}as function of the estimated parameter.

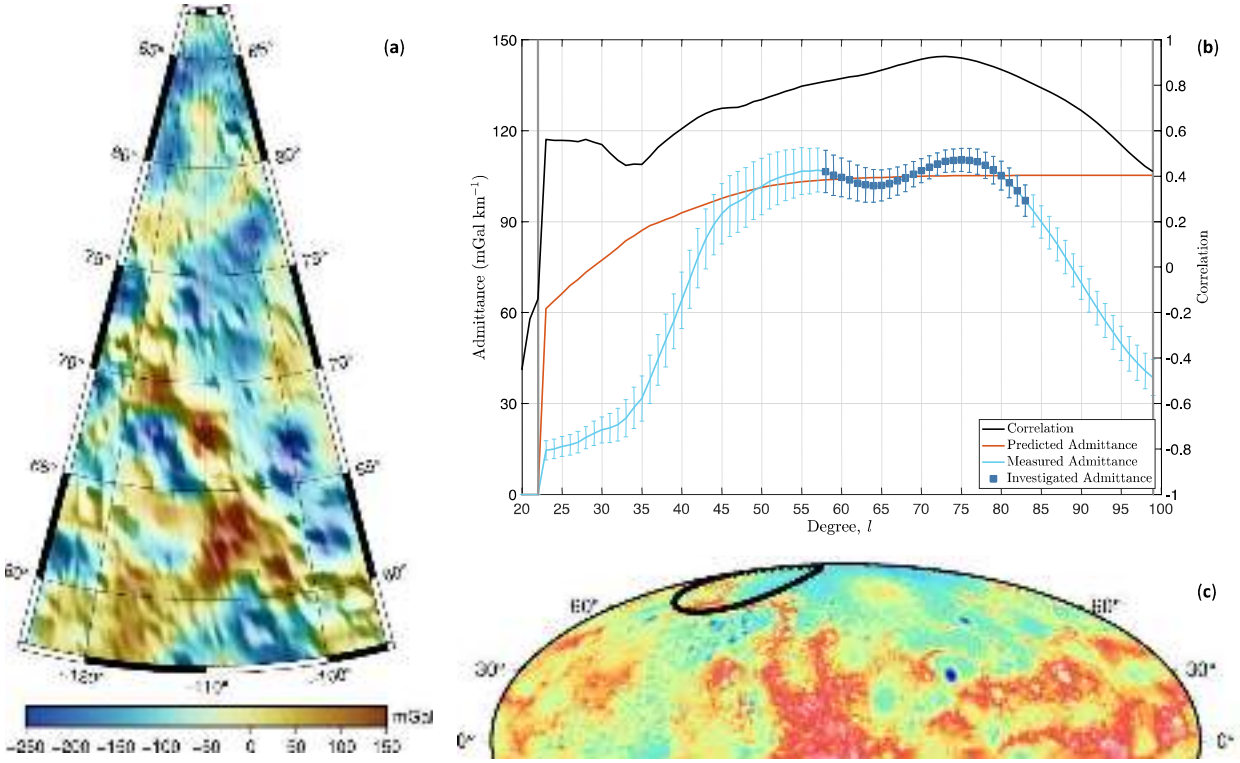

Figure 9 (**a**) Local map of free-air gravity anomaly (mGal) shown over shaded topographic relief in a Lambert Conformal Conic projection, and (**b**) correlation and admittance between gravity and topography localized on (**c**) a spherical cap centered at 250°E longitude and 72°N latitude. The localization windowing is carried out with a 15° radius, a concentration factor of 0.999 ($L_{win} = 22$), and a spherical harmonic expansion to degree $l_{max} = 121$ (see caption of Figure 3 for more details).

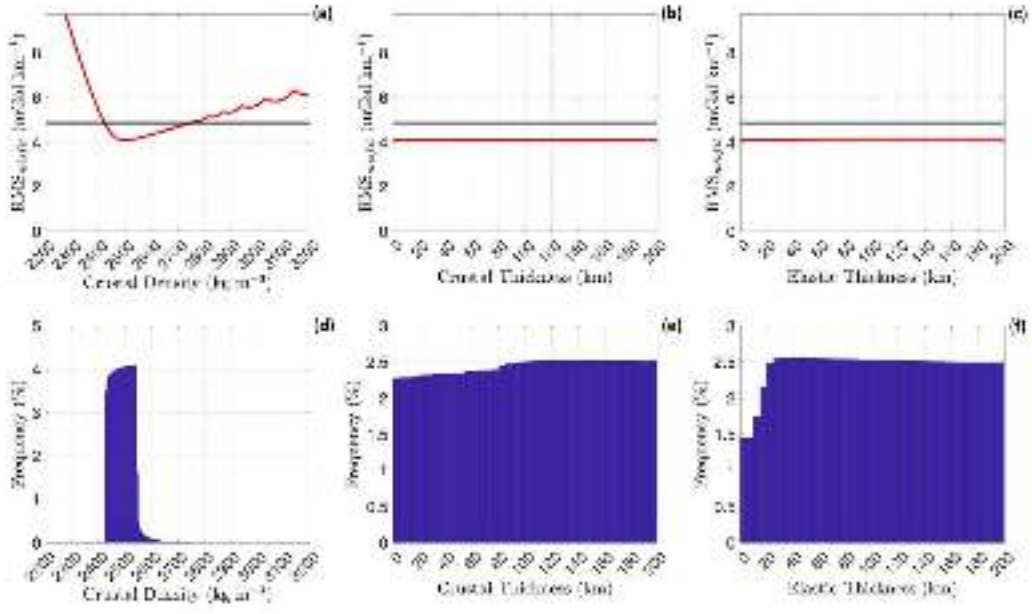

Figure 10 (**a-b-c**) Misfit plots and (**d-e-f**) histograms for the crustal density and thickness, and elastic thickness resulting from the comparison between measured and predicted localized admittance shown in Figure 9-b. The black horizontal line shows the RMS of the formal uncertainties of the local admittance, $\overline{\sigma}$, and the red curve the RMS_{misfit}as function of the estimated parameter.

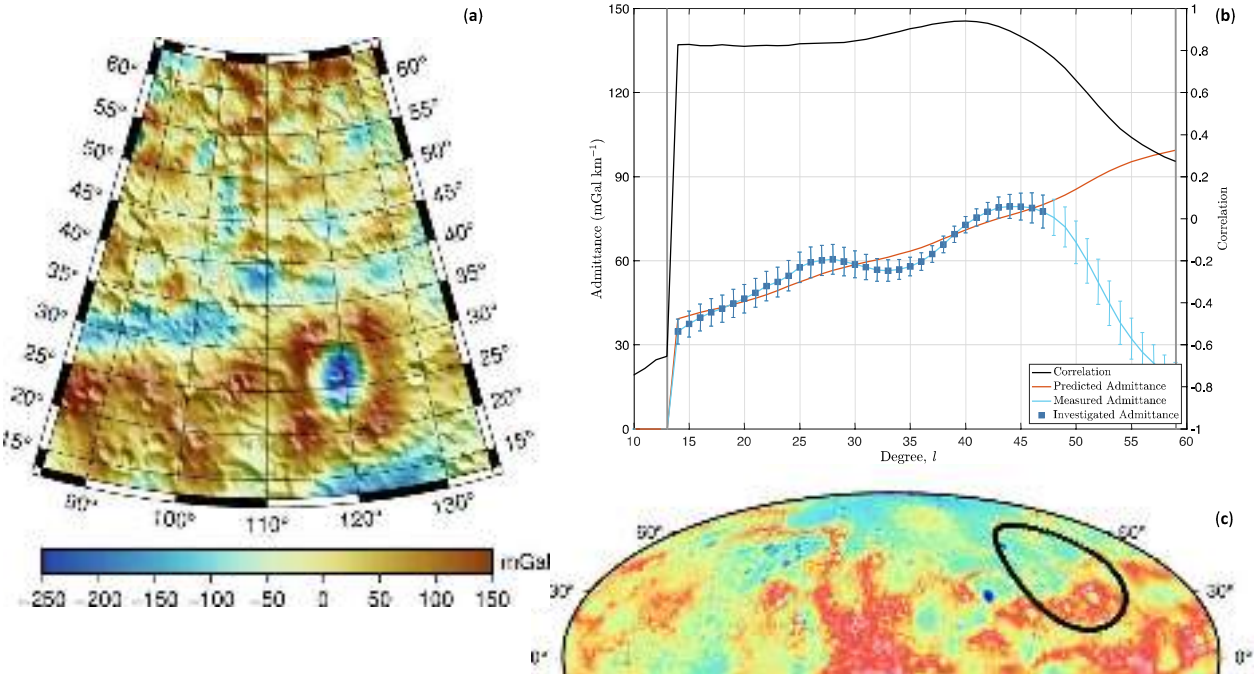

Figure 11 (**a**) Local map of free-air gravity anomaly (mGal) shown over shaded topographic relief in a Lambert Conformal Conic projection, and (**b**) correlation and admittance between gravity and topography localized on (**c**) a spherical cap centered at 110°E longitude and 38°N latitude. The localization windowing is carried out with a 25° radius, a concentration factor of 0.999 ($L_{win} = 13$), and a spherical harmonic expansion to degree $l_{max} = 72$ (see caption of Figure 3 for more details).

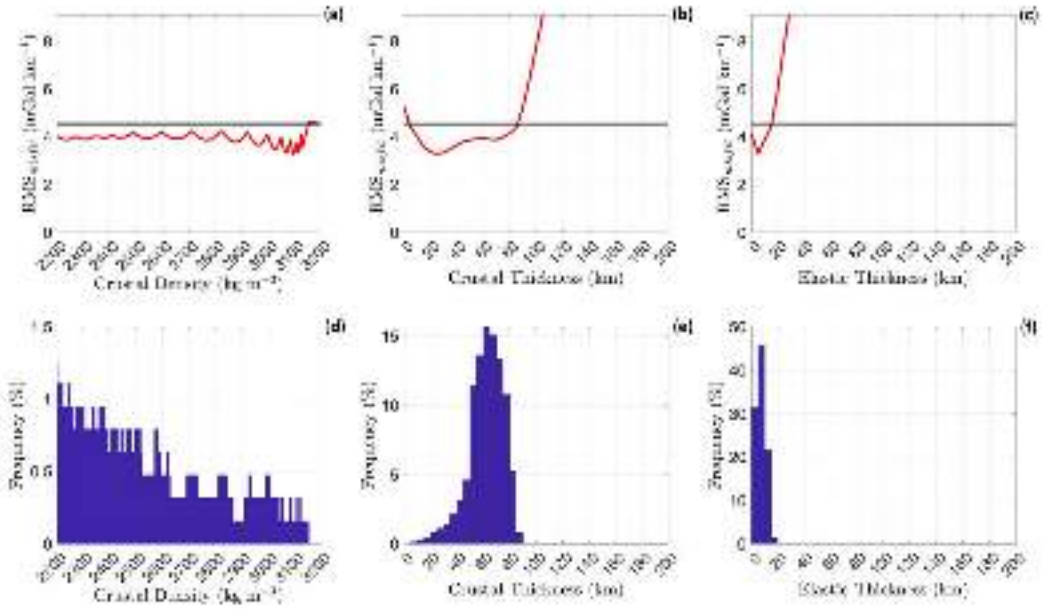

Figure 12 (**a-b-c**) Misfit plots and (**d-e-f**) histograms for the crustal density and thickness, and elastic thickness resulting from the comparison between measured and predicted localized admittance shown in Figure 11-b. The black horizontal line shows the RMS of the formal uncertainties of the local admittance, $\overline{\sigma}$, and the red curve the RMS_{misfit}as function of the estimated parameter.

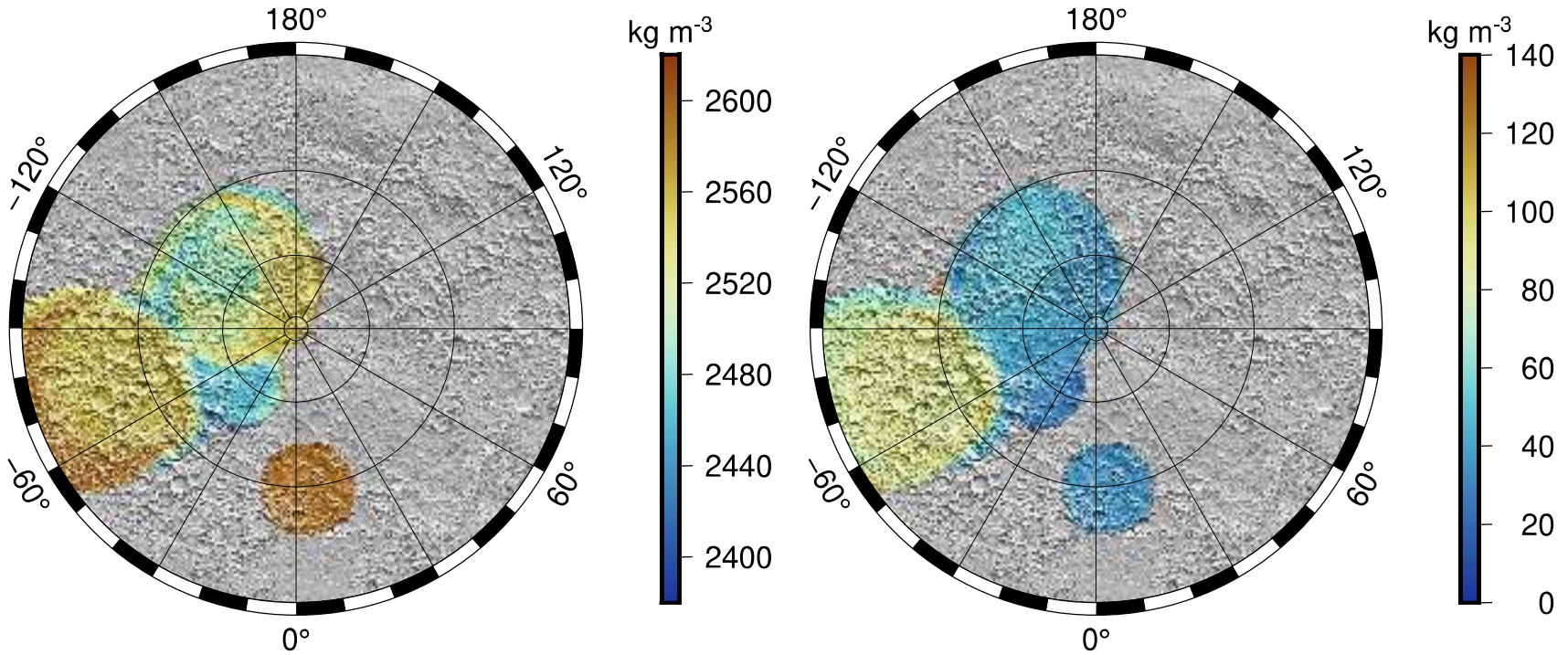

Figure 13 Maps of the lateral variations of the (**left**) crust bulk density and (**right**) its uncertainty in a polar stereographic projection from 30ºN-latitude. Grey colors show regions where the localized gravity/correlation admittance spectra do not allow to constrain the crustal density.

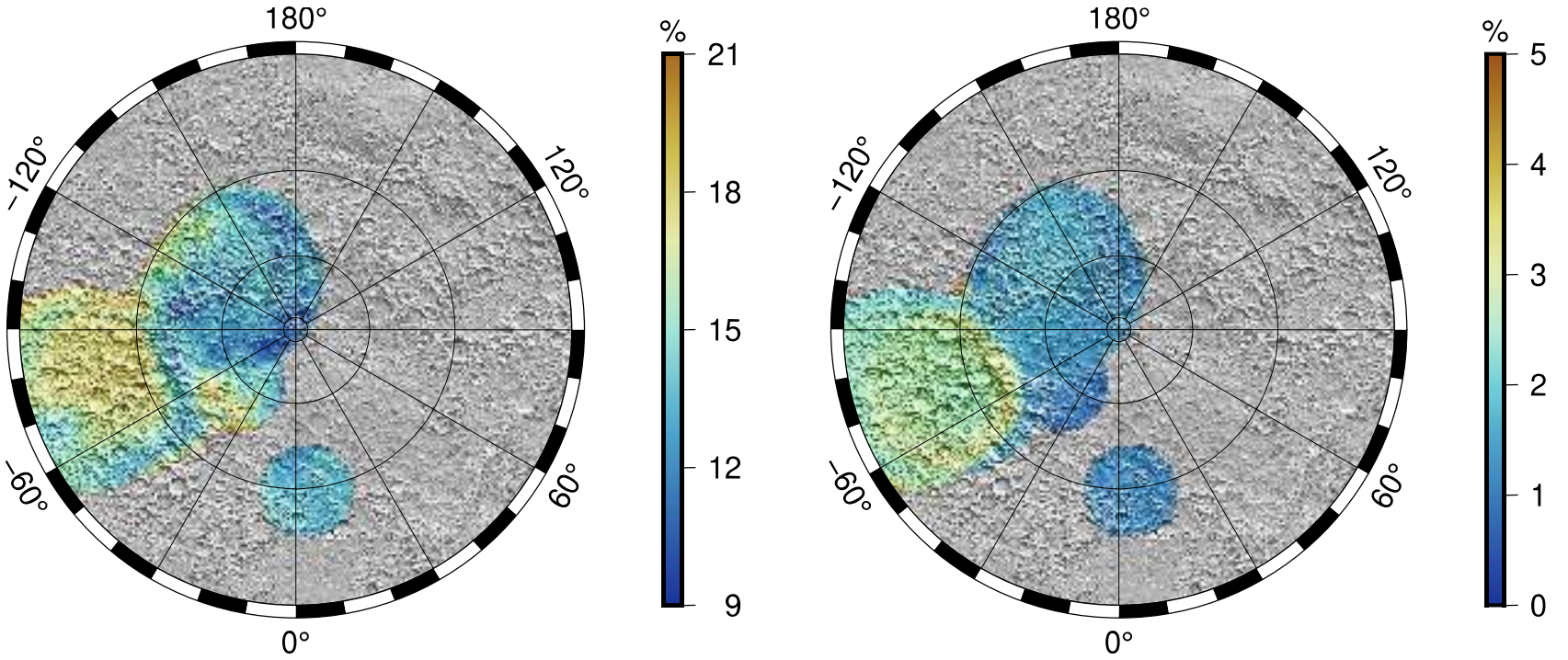

Figure 14 Maps of the lateral variations of the (**left**) surface porosity and (**right**) its uncertainty in a polar stereographic projection from 30°N-latitude. The lateral variations of the surface porosity are computed by comparing the bulk density retrieved from local admittance analyses and the grain density reported by Beuthe et al. 2020